Delocalization and scaling properties of low-dimensional quasiperiodic systems

Ai-Min Guo,[1,*] X. C. Xie,[2,3] and Qing-feng Sun[2,3,†]

[1]*Institute of Physics, Chinese Academy of Sciences, Beijing 100190, China*
[2]*International Center for Quantum Materials, Peking University, Beijing 100871, China*
[3]*Collaborative Innovation Center of Quantum Matter, Beijing 100871, China*

In this paper, we explore the localization transition and the scaling properties of both quasi-one-dimensional and two-dimensional quasiperiodic systems, which are constituted from coupling several Aubry-André (AA) chains along the transverse direction, in the presence of next-nearest-neighbor (NNN) hopping. The localization length, two-terminal conductance, and participation ratio are calculated within the tight-binding Hamiltonian. Our results reveal that a metal-insulator transition could be driven in these systems not only by changing the NNN hopping integral but also by the dimensionality effects. These results are general and hold by coupling distinct AA chains with various model parameters. Furthermore, we show from finite-size scaling that the transport properties of the two-dimensional quasiperiodic system can be described by a single parameter and the scaling function can reach the value 1, contrary to the scaling theory of localization of disordered systems. The underlying physical mechanism is discussed.

I. INTRODUCTION

Since the original prediction by Anderson that the disorder could lead to the absence of electron diffusion in imperfect crystals [1], Anderson localization has always been one of the most fascinating phenomena in condensed-matter physics and much progress has been achieved in this research field [2–5]. In fact, Anderson localization is a ubiquitous quantum phenomenon and has been directly observed in a variety of disordered systems [6–14].

On the other hand, the complementary subject of the exploration of metallic states in low-dimensional disordered systems arises and has attracted extensive attention among the physics community, in the context of electron transport and direct application of realistic materials which are always disordered. For instance, the extended states have been reported in one-dimensional (1D) disordered systems when the short- or long-range correlations are incorporated [15–19]. Another celebrated example is the Aubry-André (AA) model [20],

$$[E - W \cos(2\pi\alpha n)]\varphi_n = t(\varphi_{n-1} + \varphi_{n+1}), \qquad (1)$$

where E is the Fermi energy, W is the strength of the on-site potential, α is an irrational number and is incommensurate with the lattice, t is the nearest-neighbor hopping integral, and φ_n is the amplitude of the wave function at the nth site. Because α is irrational, the on-site potential displays quasiperiodicity and the AA model can be regarded as a quasiperiodic (QP) system.

Let us consider the commensurate case of $\alpha = p/q$ with p and q being co-prime integers. It is obvious that the resultant energy spectrum of Eq. (1) consists of q subbands and all electronic states are described by Bloch's theorem. Since an irrational number can be viewed as the ratio of

two infinite integers, the energy spectrum of the AA model splits into infinite subbands, leading to a highly fractal band structure. Besides, it has been claimed that all electronic states of the AA model are delocalized when $W < 2t$ and are exponentially localized with Lyapunov exponent $\ln(W/2t)$ when $W > 2t$ [20]. This metal-insulator transition (MIT) in parameter space has been verified experimentally in both Bose-Einstein condensates and photonic lattices. Roati *et al.* have demonstrated this phase transition for noninteracting ultracold atoms in optical lattices by studying the transport properties and both spatial and momentum distributions [10]. Lahini *et al.* have directly measured the spreading of initially narrow wave packets in photonic lattices and observed a localization phase transition at $W = 2t$ [12]. These recover the interest in the electronic properties of the AA model. Sil *et al.* have shown that a ladder network, consisting of two identical AA chains, exhibits an MIT at multiple Fermi energies in the presence of next-nearest-neighbor (NNN) hopping [21]. Biddle *et al.* have studied the localization properties of the AA chain by considering non-nearest-neighbor hopping and found the mobility edges [22,23].

Since the realistic materials usually have finite width, there is a growing interest in the localization properties of the quasi-1D system [24–30] and of the two-dimensional (2D) system in recent years [31–37]. From this perspective, it would be significant to investigate the localization transition and the scaling properties of both quasi-1D and 2D QP systems, which are made up from coupling several AA chains along the transverse direction, and there has already been one work along this research field [21]. One wonders whether there still exists an MIT in these systems in parameter space and whether the scaling theory of localization remains valid in the 2D QP system. In this paper, we will answer the above two questions and Fig. 1 plots the schematic illustration of the system contacted by two leads. By combining the Landauer-Büttiker formula with the recursive Green's-function technique, the conductance of the QP system is calculated in the presence of NNN hopping. Our results reveal that an MIT could occur in

---
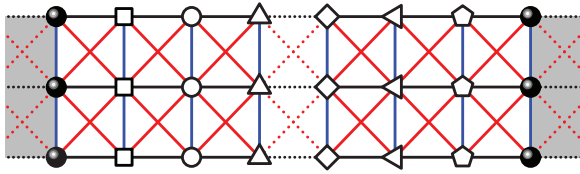*aimin.guo218@gmail.com
†sunqf@pku.edu.cn

FIG. 1. (Color online) Schematic view of the QP system (white region with open symbols) connected by two leads (gray region with filled circles). The black, blue, and red lines denote the intrachain, interchain, and NNN hopping integrals, respectively. Here, the width of the system is $S = 3$.

the quasi-1D QP system by tuning not only the NNN hopping integral but also the number of the AA chains. All of these results are general and still hold by coupling distinct AA chains with different strengths of the on-site potentials and other model parameters. In addition, we show from finite-size scaling that the transport properties of the 2D QP system can be described by a single parameter and the scaling function can reach the value 1, contrary to the scaling theory of localization. Finally, the MIT phase diagram is obtained and the statistical properties of the conductance are performed for the 2D QP system.

The rest of the paper is constructed as follows. In Sec. II, the theoretical model and the method are presented. In Sec. III, the conductance and the localization length are shown for different situations, and the scaling and statistical properties are also studied for the 2D QP system. Finally, the results are summarized in Sec. IV.

II. MODEL AND METHOD

Within the framework of the tight-binding approximation, the Hamiltonian of the QP system connected by two leads can be written as

$$\mathcal{H} = \sum_{j,n} [\varepsilon_{j,n} c_{j,n}^\dagger c_{j,n} + t c_{j,n}^\dagger c_{j,n+1} + \lambda c_{j,n}^\dagger c_{j+1,n}$$
$$+ t_d(c_{j,n}^\dagger c_{j-1,n+1} + c_{j,n}^\dagger c_{j+1,n+1}) + \text{H.c.}], \quad (2)$$

where $c_{j,n}^\dagger$ ($c_{j,n}$) creates (annihilates) an electron at lattice site (j,n) of the left lead ($n < 1$), of the central region ($1 \leqslant n \leqslant L$; white region in Fig. 1), and of the right lead ($n > L$). Here, $j \in [1, S]$ is the chain index, S is the width, and L is the length of the central region. The on-site potential $\varepsilon_{j,n}$ at the central region is set as

$$\varepsilon_{j,n} = W_j \cos(2\pi\alpha n), \quad (3)$$

with W_j the strength of the on-site potential of the jth chain and α the irrational number. t is the intrachain hopping integral and is chosen as the energy unit. λ and t_d are, respectively, the interchain and NNN hopping integrals between two neighboring chains (see Fig. 1).

The Schrödinger equation $\mathcal{H}|\Psi\rangle = E|\Psi\rangle$ in the site representation can be expressed as

$$(E\mathbf{I} - \mathcal{H}_n)\Psi_n = \mathcal{M}(\Psi_{n-1} + \Psi_{n+1}). \quad (4)$$

Here, $\mathbf{I}$ is the $S \times S$ identity matrix, $\mathcal{H}_n$ is the sub-Hamiltonian matrix of the nth layer,

$$\mathcal{H}_n = \begin{pmatrix} \varepsilon_{1,n} & \lambda & 0 & \cdots & 0 \\ \lambda & \varepsilon_{2,n} & \lambda & \ddots & \vdots \\ 0 & \lambda & \varepsilon_{3,n} & \ddots & 0 \\ \vdots & \ddots & \ddots & \ddots & \lambda \\ 0 & \cdots & 0 & \lambda & \varepsilon_{S,n} \end{pmatrix}, \quad (5)$$

$\Psi_n = (\psi_{1,n}, \psi_{2,n}, \cdots, \psi_{S,n})^T$ with $\psi_{j,n}$ the amplitude of the wave function at lattice site (j,n) and T the transpose, and $\mathcal{M}$ is the sub-Hamiltonian matrix connecting two successive layers,

$$\mathcal{M} = \begin{pmatrix} t & t_d & 0 & \cdots & 0 \\ t_d & t & t_d & \ddots & \vdots \\ 0 & t_d & t & \ddots & 0 \\ \vdots & \ddots & \ddots & \ddots & t_d \\ 0 & \cdots & 0 & t_d & t \end{pmatrix}. \quad (6)$$

At zero temperature, the Landauer conductance G can be obtained from the Landauer-Büttiker formula [38]:

$$G = G_0 \text{Tr}[\mathbf{\Gamma}_R \mathbf{G}^r \mathbf{\Gamma}_L \mathbf{G}^a], \quad (7)$$

with $G_0 = 2e^2/h$ the quantum conductance. $\mathbf{\Gamma}_{L/R} = i(\mathbf{\Sigma}_{L/R}^r - \mathbf{\Sigma}_{L/R}^a)$ is the linewidth function, $\mathbf{G}^r = (\mathbf{G}^a)^\dagger = (E\mathbf{I} - \mathbf{H} - \mathbf{\Sigma}_L^r - \mathbf{\Sigma}_R^r)^{-1}$ is the Green's function, $\mathbf{\Sigma}_{L/R}^r$ is the retarded self-energy due to the coupling to the left/right lead with the on-site potential being 0 [39], and $\mathbf{H}$ is the Hamiltonian of the central region. In the numerical calculation, the conductance can be evaluated by using the recursive Green's-function technique for very large system size. Besides, the Lyapunov exponents γ_j's are also calculated by the transfer-matrix method [26]. For the $S \times L$ system, there are S propagating channels along the longitudinal direction and each γ_j reflects the exponential decay of the corresponding channel. The smallest γ_j is the most physically significant quantity and its inverse is the localization length ξ. We emphasize that the propagating channel is distinct from the chain in Eq. (2) because of the interchain hopping integral λ and the NNN one t_d, and these two concepts are equivalent to each other when $\lambda = t_d = 0$. The fixed boundary condition is imposed in the transverse direction. In this situation, the system is closer to the realistic materials, of which their edges usually do not connect to each other, and corrections to scaling disappear faster with increasing system size [40,41].

In the following, the irrational number is taken as $\alpha = 1/(10\pi)$ and the results are usually averaged over 10^4 QP samples to reach convergence, except for specific indication in the figure caption. Each QP sample is uniformly selected from the infinite system [see Eq. (3) where the integer n can be $+\infty$ theoretically] by using the sliding window strategy [42]. For instance, the mth sample can be expressed as $\varepsilon_{j,n} = W_j \cos[2\pi\alpha(n + i*m - 1)] = W_j \cos[2\pi\alpha n + \varphi_{i,m}]$ with i and m being positive integers. Here, the integer i is chosen as $i = 1$ and the results are independent on i when the number of samples is sufficiently large.

III. RESULTS AND DISCUSSIONS

A. Delocalization induced by the NNN hopping

We first consider the case of all $W_j = W$ and prove analytically the NNN hopping-induced MIT in the QP system which is composed of several identical AA chains. In this regard, all $\mathcal{H}_n$'s and $\mathcal{M}$ can be diagonalized by applying a single unitary matrix $\mathbf{U}$ through $\mathcal{P}_n = \mathbf{U}^\dagger \mathcal{H}_n \mathbf{U}$ and $\mathcal{Q} = \mathbf{U}^\dagger \mathcal{M} \mathbf{U}$ [43]. Then, Eq. (4) can be decoupled into the following Schrödinger equations:

$$(E - \nu_{k,n})\phi_{k,n} = \mu_k(\phi_{k,n-1} + \phi_{k,n+1}), \qquad (8)$$

where $k \in [1,S]$, $(\phi_{1,n}, \phi_{2,n}, \cdots, \phi_{S,n})^T = \mathbf{U}^\dagger \mathbf{\Psi}_n$, and $\nu_{k,n}$ and μ_k are the kth eigenvalue of $\mathcal{H}_n$ and $\mathcal{M}$, respectively. In addition,

$$\nu_{k,n} = W \cos(2\pi\alpha n) + 2\lambda \cos\frac{k\pi}{S+1} \qquad (9)$$

and

$$\mu_k = t + 2t_d \cos\frac{k\pi}{S+1}. \qquad (10)$$

Accordingly, the QP system can be transformed into S isolated AA chains with identical strength W of the on-site potential [Eq. (9)] and different hopping integrals [Eq. (10)]. These decoupled chains are exactly the propagating channels as mentioned above. One can see that the interchain hopping integral only determines the positions of the energy bands of the decoupled chains and the energy bands will be farther away and even separated from each other for greater λ. In contrast, the NNN hopping integral only contributes to the hopping integrals of the decoupled chains, and some of the decoupled chains will be more delocalized with increasing t_d and contrarily the others will become more localized. Besides, we can also demonstrate the mobility edges from Eqs. (9) and (10) for the specific case $t_d = t$ [21]. It is clear that when any one of the decoupled chains has extended states, the QP system shows metallic behavior. Since the most conducting decoupled chain is the first one with $k = 1$, the critical condition to observe the MIT in the QP system is [20]

$$W_c = 2\left(t + 2t_d \cos\frac{\pi}{S+1}\right). \qquad (11)$$

When $W < W_c$, there will be at least one delocalized decoupled chain and the system exhibits metallic behavior, whereas when $W > W_c$, all of the decoupled chains are localized and the system is insulating. Although the analytical argument is performed on the special case of all $W_j = W$, we believe that the NNN hopping-induced MIT is general for other quasi-1D QP systems by coupling distinct AA chains.

To explore the generality of the NNN hopping-induced MIT in the QP system, we study the localization properties of the two-leg ladder model as an example, by coupling two distinct AA chains with different W_j's. In this situation, it is difficult to provide analytical results and the numerical calculations are performed instead. Figures 2(a)–2(c) show the localization length ξ for $t_d = 0$, $0.3t$, and $0.6t$, respectively, as a function of energy E with $W_1 = t$ and $W_2 = 4t$, while the insets display the corresponding Landauer conductance G. Here, ξ is averaged within a very small energy interval of
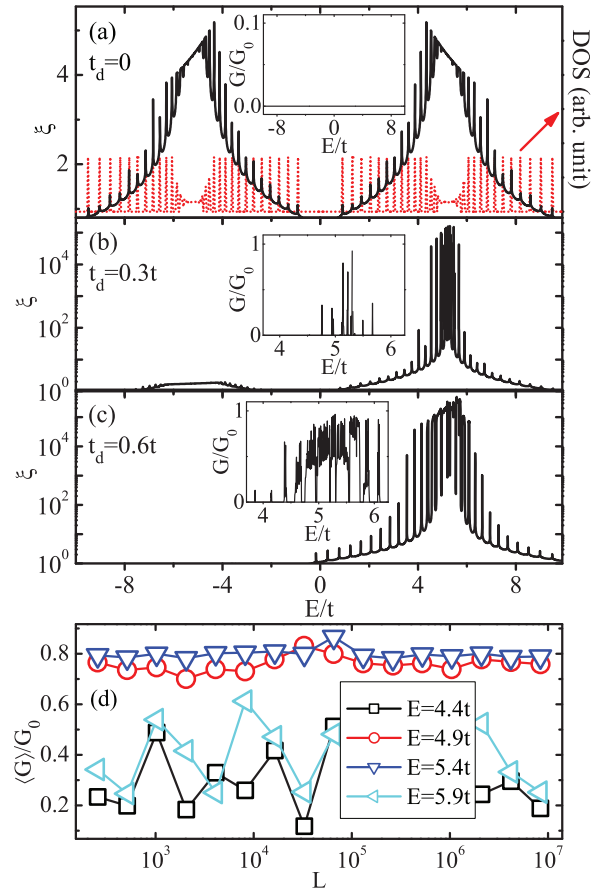

FIG. 2. (Color online) Energy-dependent localization length ξ of the two-leg ladder for (a) $t_d = 0$ (solid line), (b) $t_d = 0.3t$, and (c) $t_d = 0.6t$ with $L = 10^5$. The insets show the corresponding conductance G and the dotted line in (a) denotes the DOS. The above results are performed for a single QP sample. (d) Length-dependent averaged conductance $\langle G \rangle$ for typical values of E with $t_d = 0.6t$, which is obtained from 10^4 QP samples. Other parameters are $S = 2$, $\lambda = 5t$, $W_1 = t$, and $W_2 = 4t$.

10^{-4} to avoid numerical fluctuations. Although the localization properties of the two-leg ladder strongly depend upon the NNN hopping integral t_d (discussed later), one can see several general features that are irrespective of t_d. First, all of the energy spectra consist of two isolated subbands because of the repulsion effects between the two chains driven by the large interchain hopping integral $\lambda = 5t$ [Eq. (9)]. And these two subbands are exactly the propagating channels of the two-leg ladder. Second, there exist many sharp peaks in the curve ξ-E due to the highly fractal energy band of the AA model. This feature can be further identified in the density of states (DOS) [see the dotted line in Fig. 2(a)], which is obtained by diagonalizing the Hamiltonian of the central region, and the quantized energy levels coincide with the peaks in the curve ξ-E [Fig. 2(a)]. Here, we emphasize that the DOS profile does not change with the system length L when the two-leg ladder is sufficiently long. The origin of the extremely fractal energy spectrum can also be understood as follows: the AA model can be projected from the 2D square lattice which

develops degenerate Landau energy levels in the presence of a perpendicular magnetic field [44].

In the absence of t_d, the two subbands are almost symmetric with respect to $E = 0$ and the two-leg ladder exhibits insulating behavior with $\xi \ll L$ and $G = 0$ [see the solid line and the inset of Fig. 2(a)], although all electronic states of the first AA chain are delocalized ($W_1 = t$), consistent with a previous study in which the system composed of one disordered chain and another completely ordered chain is localized [25]. This is attributed to the fact that when an electron is injected into the first chain, it will be continuously scattered from larger (localized) potentials of the second chain, owing to the interchain hopping integral. The longer the system is, the more the scattering the electron suffers. Accordingly, G will be exponentially declined to zero with increasing L, a typical feature of Anderson localization.

While in the presence of t_d that could lead to electron-hole asymmetry, the two subbands become asymmetric and opposite behaviors could be observed with increasing t_d. For the left subband, its bandwidth decreases monotonically from $8.6t$ at $t_d = 0$ to $6.4t$ at $t_d = 0.6t$ and ξ is gradually declined by increasing t_d, and hence the electronic states become more localized. In contrast, the bandwidth of the right subband is enhanced from $8.6t$ at $t_d = 0$ to $10.8t$ at $t_d = 0.6t$ and ξ increases with t_d, and nonzero conductance could emerge in the region of large t_d [see the insets of Figs. 2(b) and 2(c)]. This phenomenon can be explained as follows. In fact, the NNN hopping integral could produce an additional two propagating channels with opposite sign of hopping integrals [Eq. (10)] and thus affect the transport properties of the two-leg ladder by mixing these channels with the original ones at $t_d = 0$. When the hopping integrals of the additional and original propagating channels are of different signs, the effective hopping integral will be reduced and leads to the shrinkage of both the bandwidth and the localization length. Contrarily, when they have identical signs, the effective hopping integral can be enhanced and both the bandwidth and the localization length can be increased, leading to a possible MIT in the two-leg ladder. Actually, the electronic states of finite conductance observed in the insets of Figs. 2(b) and 2(c) are delocalized even in the thermodynamic limit because the conductance of the localized states presents exponential dependence on the system length and should be zero when $L = 10^5$. This statement can be further verified in Fig. 2(d), where the averaged conductance $\langle G \rangle$ is plotted for several typical energies as a function of L with other parameters identical to those in Fig. 2(c). It clearly appears that $\langle G \rangle$ fluctuates around a certain value with increasing L and does not tend to zero. Therefore, we conclude that these electronic states are truly delocalized and an MIT could be driven in the two-leg ladder by increasing t_d.

To further substantiate the NNN hopping-induced MIT and the stability of the extended states in the region of large t_d, we then investigate the localization properties of the two-leg ladder with various model parameters, as illustrated in Figs. 3 and 4. First, we consider other values of W_j's, small λ, and large α. Figure 3(a) shows the conductance G versus E by coupling two localized AA chains with $W_1 = 2.2t$ and $W_2 = 3t$, while Fig. 3(b) plots G versus E for large irrational number
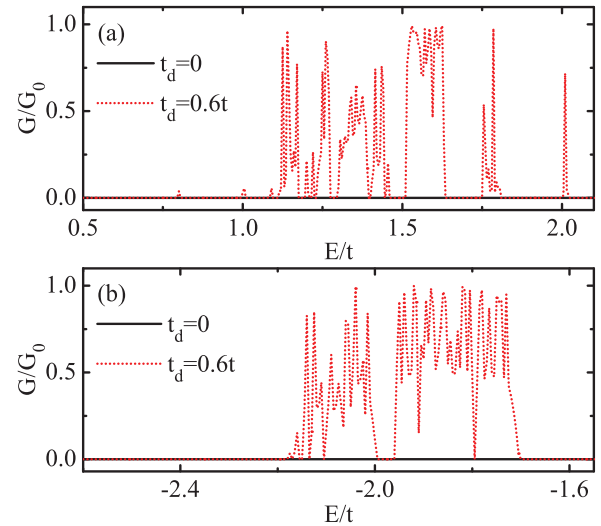

FIG. 3. (Color online) Energy-dependent G of the two-leg ladder by coupling two distinct AA chains with $t_d = 0$ (solid line) and $t_d = 0.6t$ (dotted line). (a) $W_1 = 2.2t$, $W_2 = 3t$, and $\alpha = 1/(10\pi)$. (b) $W_1 = t$, $W_2 = 4t$, and $\alpha = (1 + \sqrt{5})/2$. Other parameters are $S = 2$, $L = 10^5$, and $\lambda = t$. The results are calculated from a single QP sample.
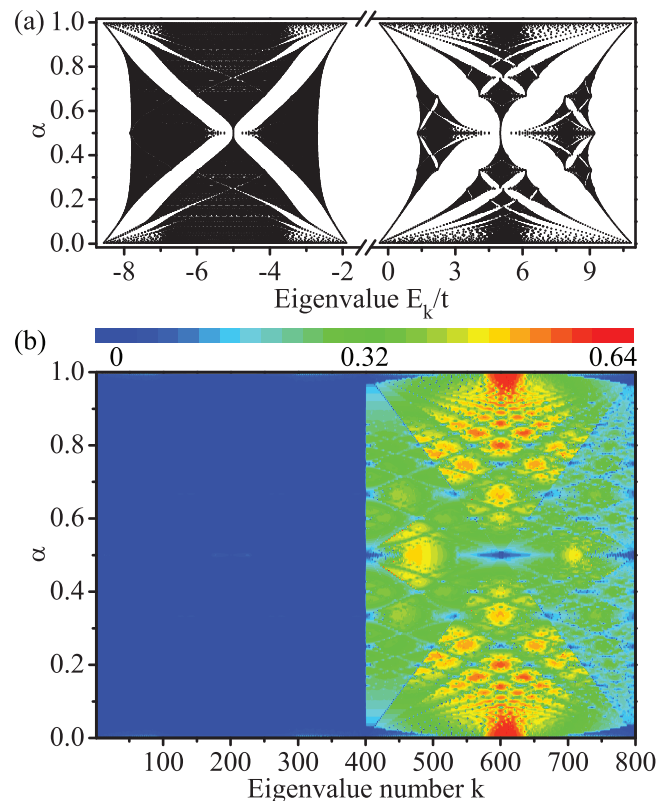

FIG. 4. (Color online) (a) Eigenvalue spectrum of the two-leg ladder by varying the irrational number α within $(0,1)$. (b) 2D plot of P_r vs the eigenvalue number k [see the horizontal coordinate E_k in (a)] and α. Larger k refers to higher E_k. Here, $L = 400$ and other parameters are the same as those in Fig. 2(c). All of these results are performed for a single QP sample and are similar when other QP samples are considered or by coupling two identical AA chains with $W_1 = W_2$.

$\alpha = (1 + \sqrt{5})/2$, with the small interchain hopping integral $\lambda = t$. It can be seen that all electronic states are localized with $G = 0$ in the absence of t_d [see the solid lines in Figs. 3(a) and 3(b)] and the extended states of nonzero conductance could emerge when t_d becomes large [see the dotted lines in Figs. 3(a) and 3(b)]. Since the band structure of the two-leg ladder is sensitive to both α and W_j's, the position of the extended states is distinct from each other when α or W_j is different.

Second, we consider the irrational number α within a wide range. Figure 4(a) plots the eigenvalue spectrum of the two-leg ladder by changing α from 0 to 1. It clearly appears that there exist two Hofstadter-like butterflies in the energy spectrum, although the system is composed of two distinct AA chains with different W_j's. The left subband exhibits the compressed configuration of the Hofstadter's butterfly due to the small width $6.7t$ (the original Hofstadter's butterfly was reported at $W = 2t$ with width $8t$) [44], and the right subband shows the expanded version with width $11.2t$.

To illustrate the localization properties at different α, it is convenient to calculate the participation ratio P_r [5]:

$$P_r = \frac{1}{SL \sum_{j=1}^{S} \sum_{n=1}^{L} |\psi_{j,n}|^4},$$ (12)

which measures the extension of the wave function. Figure 4(b) shows the corresponding 2D plot of P_r versus the eigenvalue number k and α. It can be seen that P_r is very small in the left subband ($1 \leqslant k \leqslant 400$) and the wave functions are confined within a small region. Our further calculations reveal that P_r decreases with increasing L, indicating that all electronic states are localized in the left subband [26]. In contrast, P_r is usually very large in the right subband ($401 \leqslant k \leqslant 800$) and the wave functions can spread over the entire system for all investigated values of α, except for some electronic states which locate at the band edge and the corresponding P_r remains quite small [see the four corners of the right subband in Fig. 4(b)]. The small P_r in these corners may originate from the fact that (1) the QP character of the system is not obvious for short system length $L = 400$ when α is very close to an integer and (2) the electronic states in the band edge are isolated from others and cannot form a band, and thus become fragile. However, we find that the large P_r is independent on L (data not shown), implying that the corresponding electronic states are delocalized in the right subband. Besides, one can see that P_r exhibits clustering patterns in the right subband and is extremely large within these regions, owing to the highly degenerate energy levels. Therefore, our results demonstrate that the extended states still exist in the case of large t_d for all investigated values of W_j, λ, and α, and thus the NNN hopping-induced MIT is general. Since the localization properties of the system do not depend upon λ, in the following we fix the interchain hopping integral as $\lambda = t$ without loss of generality.

B. Delocalization induced by the dimensionality

Besides the NNN hopping, it can be seen from Eq. (10) that the hopping integrals of some decoupled chains can be enhanced with increasing the system width S in the presence of t_d and the extended states can emerge in the case of large S when $W < W_c$. Figure 5(a) displays the conductance G versus E for several quasi-1D QP systems which are
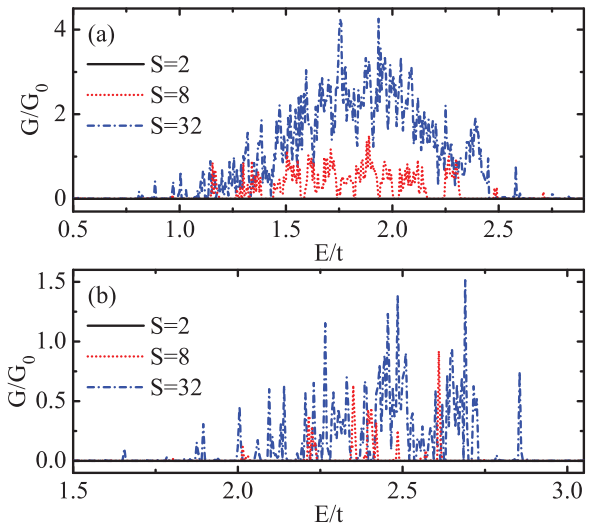

FIG. 5. (Color online) G vs E of several quasi-1D QP systems with different width S. (a) $W_j = 2.4t$ for all j's. (b) $W_j = t$ when j is odd and $W_j = 4t$ when j is even. Other parameters are $L = 10^5$, $\lambda = t$, and $t_d = 0.2t$. The results are performed for a single QP sample.

composed of identical AA chains with all $W_j = 2.4t$ and $L = 10^5$. One notices that G is zero within the numerical accuracy for $S = 2$ [see the solid line of Fig. 5(a)] and is progressively increased with increasing S as expected [see the dotted and dash-dotted lines of Fig. 5(a)], implying the occurrence of MIT in the quasi-1D QP systems. The underlying physics for the extended states observed in large S can be ascribed to the dimensionality effects together with the NNN hopping. Just like the two-leg ladder model, the NNN hopping integral could also generate additional propagating channels with various hopping integrals in the quasi-1D systems [Eq. (10)]. These additional propagating channels will interact with the original ones at $t_d = 0$ and change the transport properties of the quasi-1D system with both localized and delocalized channels. Since both the number of the delocalized channels and the conductance of the original ones increase with S, the system's conductance can become larger with increasing S. The dimensionality-effects-induced MIT is a general phenomenon and can still take place in the QP systems by coupling distinct AA chains of different W_j's, as illustrated in Fig. 5(b), where the conductance G is shown for several quasi-1D QP systems by coupling two kinds of AA chains. Besides, the conductance profiles exhibit several gaps for small S [see the dotted lines of Figs. 5(a) and 5(b)] and these gaps tend to disappear for large S because the energy spectra of the delocalized channels are different and can distribute over a wide energy range with increasing S. Therefore, we conclude that an MIT could also be driven in the quasi-1D QP systems by increasing the system width.

C. Localization properties of the 2D QP system and the phase diagram

We then study the localization phase transition and the scaling properties of the 2D QP system with $L = S$. For the purpose of scaling, the contact resistance is subtracted from G to yield the Thouless conductance g, which is expressed
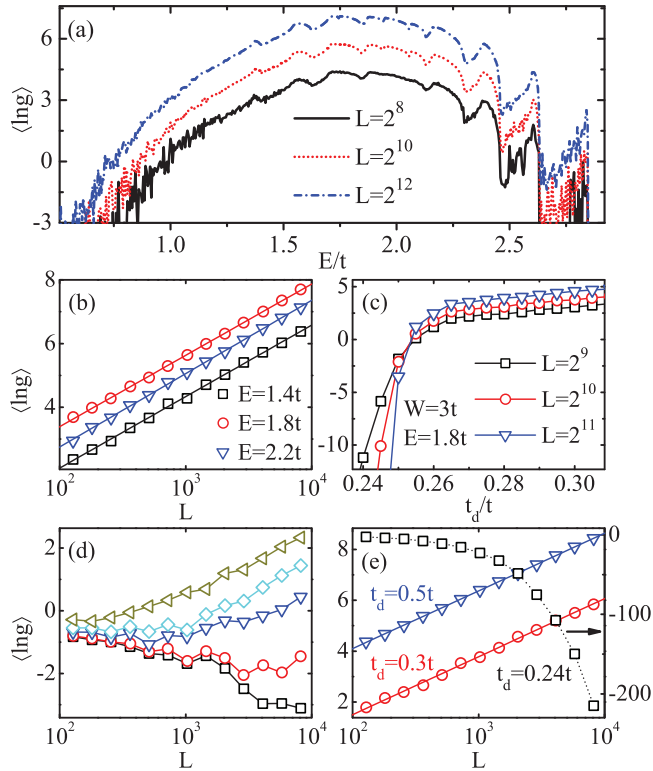
FIG. 6. (Color online) Scaling properties of $\langle \ln g \rangle$ for the 2D QP system with $S = L$ and all $W_j = W$. (a) $\langle \ln g \rangle$ vs E for different L and (b) $\langle \ln g \rangle$ vs L for several values of E with $W = 2.4t$ and $t_d = 0.2t$. (c) $\langle \ln g \rangle$ vs t_d for distinct L, (d) $\langle \ln g \rangle$ vs L for various t_d which is very close to the critical value t_d^c (see text), and (e) $\langle \ln g \rangle$ vs L for several t_d which is distant from t_d^c, by fixing $W = 3t$ and $E = 1.8t$. (d) The squares, circles, down triangles, diamonds, and left triangles denote $t_d = 0.2508t, 0.251t, 0.252t, 0.253t$, and $0.255t$, respectively. (e) The circles and down triangles represent, respectively, $t_d = 0.3t$ and $0.5t$ with their vertical axis on the left side, while the squares correspond to $t_d = 0.24t$ with its vertical axis on the right side (as indicated by the arrow). (b),(e) The solid lines are the linear fitting curves $\langle \ln g \rangle \propto \beta_0 \ln L$ with β_0 being about 1. The results are averaged over 10^4 QP samples.

as [38,41]

$$\frac{1}{g} = \frac{G_0}{2G} - \frac{1}{2N}. \tag{13}$$

Here, N is the number of propagating channels in the leads at Fermi energy E with $1/(2N)$ the contact resistance. Then, the scaling function [2,41],

$$\beta = \frac{d \langle \ln g \rangle}{d \ln L}, \tag{14}$$

is numerically evaluated and is used to determine the localization and scaling properties. $\beta < 0$ and $\beta > 0$ correspond to the insulator and the metal, respectively.

Figure 6(a) shows the energy-dependent $\langle \ln g \rangle$ for the 2D QP system with several values of L. It can be seen that $\langle \ln g \rangle$ increases with L in a wide energy range and exhibits strong fluctuations in the band edge, owing to the fractal energy spectrum of the AA model. The scaling behavior of $\langle \ln g \rangle$ on L is plotted in Fig. 6(b) for several typical energies. It

clearly appears that $\langle \ln g \rangle$ increases monotonically with L and the dependence of $\langle \ln g \rangle$ on L can be well fitted by a simple function $\langle \ln g \rangle \propto \beta_0 \ln L$, with the exponent β_0 being about 1. This implies that the 2D QP system presents truly metallic behavior in the thermodynamic limit.

Figure 6(c) displays $\langle \ln g \rangle$ versus t_d for several L. One can see that $\langle \ln g \rangle$ increases with t_d, which is due to the emergence of additional delocalized channels and the enhancement of the conductance of the original ones in the 2D system. Besides, the curves $\langle \ln g \rangle$-t_d for different L intersect at a critical value t_d^c of the NNN hopping integral. For $t_d < t_d^c$, $\langle \ln g \rangle$ decreases with L and corresponds to the localized regime; whereas for $t_d > t_d^c$, $\langle \ln g \rangle$ increases with L and the system is in the metallic regime. This feature can be further observed in Figs. 6(d) and 6(e), where $\langle \ln g \rangle$ is shown as a function of L with t_d close to and distant from the critical value t_d^c, respectively. It can be seen that there exist fluctuations in the curve $\langle \ln g \rangle$-L in the region of small conductance [see the squares, circles, and down triangles in Fig. 6(d)]. The curve $\langle \ln g \rangle$-L is smooth in the region of large conductance [see the left triangles in Fig. 6(d)] and can also be fitted well by the function $\langle \ln g \rangle \propto \beta_0 \ln L$ with $\beta_0 \approx 1$ when $\langle \ln g \rangle$ becomes larger [see the circles and down triangles in Fig. 6(e)].

Figure 7 plots the scaling function β versus $\langle \ln g \rangle$ and the bottom inset shows the dependence of $\langle \ln g \rangle$ on the sample number N_S for typical parameters. It clearly appears that the oscillating amplitude of $\langle \ln g \rangle$ declines quickly with increasing N_S and $\langle \ln g \rangle$ saturates when $N_S > 300$ (see the bottom inset of Fig. 7). For instance, the ratio of the difference between $\langle \ln g \rangle$ at $N_S = 294$ and its saturated value to the saturated value is 0.08%, where the saturated value of $\langle \ln g \rangle$ is prescribed at $N_S = 10^5$. Here, β is calculated from 10^4 samples to avoid spurious effects and the length is taken as $L > 10^2$ to capture
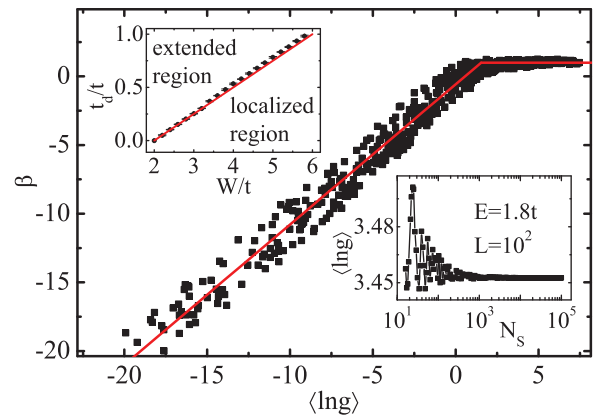

FIG. 7. (Color online) Scaling function β vs $\langle \ln g \rangle$ for the 2D QP system. β is calculated from a wide range of W, t_d, and E. Here, the length is taken as $L > 10^2$ to capture the QP character of the system, the step of the length is chosen as $d \ln L = 0.2$, and 10^4 QP samples are considered. The oblique line is the fitting curve of $\beta \propto 1.02 \langle \ln g \rangle$ for $\langle \ln g \rangle < 0$ and the horizontal line is $\beta = 1$. The top inset displays the MIT phase diagram in the W-t_d space (black symbols), which is extracted from Fig. 6(c), and the solid line denotes the curve $W = 2(t + 2t_d)$. The bottom inset shows $\langle \ln g \rangle$ as a function of the sample number N_S with $E = 1.8t$, $L = 10^2$, and other parameters being identical to those in Fig. 6(a).

the QP character of the system. It can be seen from Fig. 7 that all data points tend to construct a single curve of $\beta - \langle \ln g \rangle$. For small conductance, the scaling function can be linearly fitted by a simple function $\beta \propto 1.02 \langle \ln g \rangle$ (see the oblique line), in good agreement with the scaling theory of localization [2], implying that the conductance falls off exponentially with increasing L in the localized regime. For large conductance, the scaling function is approximately 1 (see the horizontal line of $\beta = 1$), indicating that the conductance increases linearly with L. This point is contrary to the scaling theory of localization that the scaling function should be less than 0 for the 2D disordered systems [2]. The underlying physics can be attributed to the fact that the system we studied is QP, but not disordered. In this situation, the delocalized channels as well as their conductances will be increased by increasing L.

However, there exist fluctuations in the curve $\beta - \langle \ln g \rangle$, especially in the regime of small conductance. This phenomenon is mainly due to the highly fractal energy spectrum of the QP system. One can see from Fig. 6(a) that $\langle \ln g \rangle$ fluctuates very strongly for small $\langle \ln g \rangle$, in sharp contrast to the situation where it is smooth for large $\langle \ln g \rangle$, for whatever the system size is. These fluctuations can also be identified in Fig. 6(d), as discussed above. The top inset of Fig. 7 displays the MIT phase diagram in the W-t_d space (see the black symbols), which is subtracted from Fig. 6(c). It can be seen that the critical NNN hopping integral t_d to observe metallic states increases monotonically with W and the curve of t_d-W can be fitted by $W = 2(t + 2t_d)$.

D. Statistical properties of the 2D system

Finally, we investigate the statistical properties of the Thouless conductance of the 2D QP system. Figures 8(a) and 8(b) show, respectively, the distribution of g for typical parameters and the energy-dependent standard deviation $\sigma_g =$
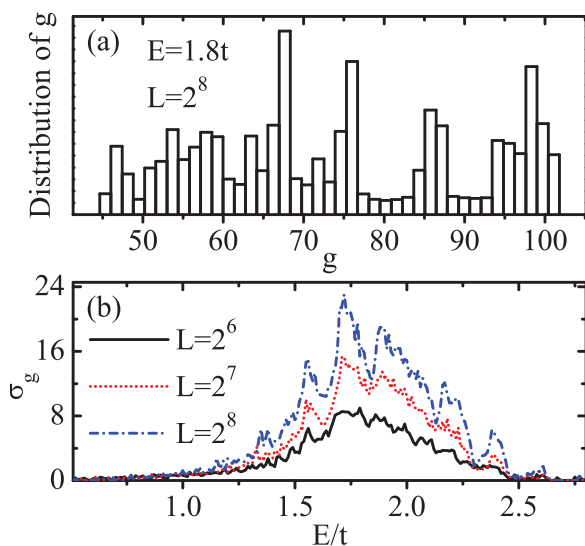

FIG. 8. (Color online) Statistical properties of the Thouless conductance for the 2D QP system. (a) Distribution of g and (b) energy-dependent standard deviation $\sigma_g = \sqrt{\langle g^2 \rangle - \langle g \rangle^2}$. The results are obtained from 10^5 QP samples and other parameters are identical to those in Fig. 6(a).

$\sqrt{\langle g^2 \rangle - \langle g \rangle^2}$ for three system sizes with $N_S = 10^5$. It can be seen from Fig. 8(a) that the distribution of g is extremely complicated and is not normal, which is different from previous studies in disordered systems [40,45]. Because of the cosine modulation of the on-site energies and the quasiperiodicity, we find that the conductance presents oscillating behavior with various amplitudes when the sample is successively chosen from an infinite AA chain by using the sliding window strategy (data not shown). Besides, we can see that the probability is quite large or small when the conductance is around specific values. As a result, the distribution of g will deviate from the normal one.

By inspecting Fig. 8(b), one notices the following features: (1) The magnitude of σ_g is comparable to $\langle g \rangle$ [see Fig. 6(a) and $\exp(\langle \ln g \rangle)$ can be viewed as an approximation of $\langle g \rangle$], where σ_g is large around the band center and becomes very small within the band edge. It can also be observed that σ_g becomes greater when $\langle g \rangle$ is larger, indicating that the fluctuation of the conductance will be stronger for larger conductance. (2) σ_g is enhanced by increasing L around the band center, where the conductance increases with L [see Fig. 6(a)] and the system presents metallic behavior. This is different from the universal conductance fluctuation theory that σ_g should be independent of the system size. (3) There are several dips in the profile of $\sigma_g - E$, similar to that observed in Fig. 6(a).

IV. CONCLUSIONS

In summary, we investigate the localization phase transition and the scaling properties of both quasi-one-dimensional and two-dimensional quasiperiodic systems, which are constructed by coupling several Aubry-André chains along the transverse direction. By employing the Landauer-Büttiker formula and the recursive Green's-function method, the two-terminal conductance is calculated for the quasiperiodic systems with next-nearest-neighbor hopping. The numerical results indicate that a metal-insulator transition could be produced in these quasiperiodic systems in parameter space by adjusting the next-nearest-neighbor hopping integral and the number of chains. These results are general and hold by coupling distinct AA chains with different strengths of the on-site potentials and other model parameters. We find that the energy spectrum of the two-leg ladder model exhibits two Hofstadter-like butterflies. Besides, we show from the finite-size scaling that the transport properties of the two-dimensional quasiperiodic system can be described by the single Thouless conductance and the scaling function can reach the value 1, contrary to the scaling theory of localization.

[1] P. W. Anderson, Phys. Rev. **109**, 1492 (1958).

[2] E. Abrahams, P. W. Anderson, D. C. Licciardello, and T. V. Ramakrishnan, Phys. Rev. Lett. **42**, 673 (1979).

[3] F. Evers and A. D. Mirlin, Rev. Mod. Phys. **80**, 1355 (2008).

[4] *50 Years of Anderson Localization*, edited by E. Abrahams (World Scientific, Singapore, 2010).

[5] S. Johri and R. N. Bhatt, Phys. Rev. Lett. **109**, 076402 (2012).

[6] T. Schwartz, G. Bartal, S. Fishman, and M. Segev, Nature (London) **446**, 52 (2007).

[7] Y. Lahini, A. Avidan, F. Pozzi, M. Sorel, R. Morandotti, D. N. Christodoulides, and Y. Silberberg, Phys. Rev. Lett. **100**, 013906 (2008).

[8] H. Hu, A. Strybulevych, J. H. Page, S. E. Skipetrov, and B. A. van Tiggelen, Nat. Phys. **4**, 945 (2008).

[9] J. Billy, V. Josse, Z. Zuo, A. Bernard, B. Hambrecht, P. Lugan, D. Clément, L. Sanchez-Palencia, P. Bouyer, and A. Aspect, Nature (London) **453**, 891 (2008).

[10] G. Roati, C. D'Errico, L. Fallani, M. Fattori, C. Fort, M. Zaccanti, G. Modugno, M. Modugno, and M. Inguscio, Nature (London) **453**, 895 (2008).

[11] S. Faez, A. Strybulevych, J. H. Page, A. Lagendijk, and B. A. van Tiggelen, Phys. Rev. Lett. **103**, 155703 (2009).

[12] Y. Lahini, R. Pugatch, F. Pozzi, M. Sorel, R. Morandotti, N. Davidson, and Y. Silberberg, Phys. Rev. Lett. **103**, 013901 (2009).

[13] S. S. Kondov, W. R. McGehee, J. J. Zirbel, and B. DeMarco, Science **334**, 66 (2011).

[14] F. Jendrzejewski, A. Bernard, K. Müller, P. Cheinet, V. Josse, M. Piraud, L. Pezzé, L. Sanchez-Palencia, A. Aspect, and P. Bouyer, Nat. Phys. **8**, 398 (2012).

[15] F. A. B. F. de Moura and M. L. Lyra, Phys. Rev. Lett. **81**, 3735 (1998).

[16] V. Bellani, E. Diez, R. Hey, L. Toni, L. Tarricone, G. B. Parravicini, F. Domínguez-Adame, and R. Gómez-Alcalá, Phys. Rev. Lett. **82**, 2159 (1999).

[17] F. M. Izrailev and A. A. Krokhin, Phys. Rev. Lett. **82**, 4062 (1999).

[18] U. Kuhl, F. M. Izrailev, A. A. Krokhin, and H.-J. Stöckmann, Appl. Phys. Lett. **77**, 633 (2000).

[19] F. M. Izrailev, A. A. Krokhin, and N. M. Makarov, Phys. Rep. **512**, 125 (2012).

[20] S. Aubry and G. André, Ann. Israel Phys. Soc. **3**, 133 (1980).

[21] S. Sil, S. K. Maiti, and A. Chakrabarti, Phys. Rev. Lett. **101**, 076803 (2008).

[22] J. Biddle and S. Das Sarma, Phys. Rev. Lett. **104**, 070601 (2010).

[23] J. Biddle, D. J. Priour, Jr., B. Wang, and S. Das Sarma, Phys. Rev. B **83**, 075105 (2011).

[24] F. A. B. F. de Moura, R. A. Caetano, and M. L. Lyra, Phys. Rev. B **81**, 125104 (2010).

[25] W. Zhang, R. Yang, Y. Zhao, S. Duan, P. Zhang, and S. E. Ulloa, Phys. Rev. B **81**, 214202 (2010).

[26] A.-M. Guo and S.-J. Xiong, Phys. Rev. B **83**, 245108 (2011).

[27] H.-Y. Xie, V. E. Kravtsov, and M. Müller, Phys. Rev. B **86**, 014205 (2012).

[28] J. J. Krich and A. Aspuru-Guzik, Phys. Rev. Lett. **106**, 156405 (2011).

[29] T. A. Sedrakyan, J. P. Kestner, and S. Das Sarma, Phys. Rev. A **84**, 053621 (2011).

[30] A. Rodriguez, A. Chakrabarti, and R. A. Römer, Phys. Rev. B **86**, 085119 (2012).

[31] M. Hilke, Phys. Rev. Lett. **91**, 226403 (2003).

[32] A. Punnoose and A. M. Finkel'stein, Science **310**, 289 (2005).

[33] M. Onoda, Y. Avishai, and N. Nagaosa, Phys. Rev. Lett. **98**, 076802 (2007).

[34] J. H. Bardarson, J. Tworzydło, P. W. Brouwer, and C. W. J. Beenakker, Phys. Rev. Lett. **99**, 106801 (2007).

[35] K. Nomura, M. Koshino, and S. Ryu, Phys. Rev. Lett. **99**, 146806 (2007).

[36] Y.-Y. Zhang, J. Hu, B. A. Bernevig, X. R. Wang, X. C. Xie, and W. M. Liu, Phys. Rev. Lett. **102**, 106401 (2009).

[37] Z. Xu, L. Sheng, R. Shen, B. Wang, and D. Y. Xing, J. Phys.: Condens. Matter **25**, 065501 (2013).

[38] *Electronic Transport in Mesoscopic Systems*, edited by S. Datta (Cambridge University Press, Cambridge, UK, 1995).

[39] D. H. Lee and J. D. Joannopoulos, Phys. Rev. B **23**, 4997 (1981).

[40] K. Slevin, T. Ohtsuki, and T. Kawarabayashi, Phys. Rev. Lett. **84**, 3915 (2000).

[41] K. Slevin, P. Markoš, and T. Ohtsuki, Phys. Rev. Lett. **86**, 3594 (2001).

[42] A.-M. Guo and S.-J. Xiong, Phys. Rev. E **79**, 041924 (2009).

[43] A.-M. Guo, S.-J. Xiong, X. C. Xie, and Q.-F. Sun, J. Phys.: Condens. Matter **25**, 415501 (2013).

[44] D. R. Hofstadter, Phys. Rev. B **14**, 2239 (1976).

[45] K. Slevin, Y. Asada, and L. I. Deych, Phys. Rev. B **70**, 054201 (2004).